Double Wall Carbon Nanotubes for Wide-Band, Ultrafast Pulse Generation

Tawfique Hasan[1,], Zhipei Sun[2], PingHeng Tan[3], Daniel Popa[1], Emmanuel Flahaut[4,5], Edmund J. R. Kelleher[6], Francesco Bonaccorso[7,8], Fengqiu Wang[9], Zhe Jiang[1], Felice Torrisi[1], Giulia Privitera[1], Valeria Nicolosi[10] and Andrea C. Ferrari[1]*

[1] Cambridge Graphene Centre, University of Cambridge, Cambridge, CB3 0FA, UK

[2] Department of Micro- and Nanosciences, Aalto University, FI-00076 Aalto, Finland

[3] State Key Laboratory for Supearlattices and Microstructures, P. O. Box 912, Beijing 100083, China

[4] Université de Toulouse; UPS, INP; Institut Carnot Cirimat; Toulouse cedex 9, France

[5] CNRS ; Institut Carnot Cirimat; F-31062 Toulouse, France

[6] Femtosecond Optics Group, Department of Physics, Imperial College, SW7 2AZ, UK

[7] CNR-Istituto Processi Chimico-Fisici, 98158 Messina, Italy

[8] NEST, Istituto Nanoscienze-CNR and Scuola Normale Superiore, I-56126 Pisa, Italy

[9] School of Electronic Science and Engineering, Nanjing University, Nanjing, 210023, China

[10] School of Chemistry, School of Physics, CRANN and AMBER, Trinity College Dublin, D2, Ireland

KEYWORDS: Double Wall Carbon Nanotubes, Polymer Composites, Saturable Absorber, Ultrafast Laser.

ABSTRACT: We demonstrate wideband ultrafast optical pulse generation at 1, 1.5 and 2μm using a single polymer composite saturable absorber based on Double-Wall Carbon Nanotubes (DWNT). The freestanding optical quality polymer composite is prepared from nanotubes dispersed in water with polyvinyl alcohol as the host matrix. The composite is then integrated into Ytterbium- (Yb-), Erbium- (Er-) and Thulium- (Tm-) doped fiber laser cavities. Using this single DWNT-polymer composite, we achieve 4.85ps, 532fs and 1.6ps mode-locked pulses at 1066, 1559 and 1883nm, respectively, highlighting the potential of DWNTs for wideband ultrafast photonics.

Materials with nonlinear optical properties are of critical importance for a diverse range of photonic applications,[1] *e.g.,* optical regeneration,[2-4] switching,[2, 5, 6] modulation,[7, 8] sampling[9, 10] and noise suppression.[11] In this field, one of the most sought-after applications involves generation of ultrafast laser pulses.[12, 13] Indeed, laser sources producing nano to sub-picosecond optical pulses are a major component in the product portfolio of leading laser manufacturers.[12] Many of the relevant applications, ranging from basic scientific research to materials processing, from eye surgery to printed circuit board manufacturing, from metrology to trimming of electronic components (*e.g.*, resistors and capacitors) currently employ laser sources utilizing a mode-locking technique based on a nonlinear optical material, called saturable absorber (SA). These SAs, when placed in a laser cavity, modify the laser continuous-wave output into a train of ultrashort optical pulses.[12] The key requirements for such nonlinear optical materials are fast response time, large nonlinearity, broad wavelength range, low optical loss, high power handling, low cost and ease of integration into an optical system.[12] Currently, the dominant commercial SA technology is based on semiconductor saturable absorber mirrors (SESAMs).[14] However, these typically have limited operation bandwidths (a few tens of nanometers[12, 13]), and require complex fabrication and packaging.[12] A simpler and cost-effective alternative relies on using Single Wall Carbon Nanotubes (SWNTs)[15-28] or graphene.[15, 28-40] While broadband operation in SWNT-based devices can be achieved using a distribution of tube diameters,[15, 21, 28, 41, 42] this is an intrinsic property of graphene, due to the gapless linear dispersion of Dirac electrons.[31, 42, 43]

In general, a good SA should have a high (*e.g.*, ~10% for fiber lasers[13]) modulation depth (the absorption change between high and low intensity optical irradiation).[12, 42] However, for a pristine single layer graphene device, the optical absorption is relatively low (~2.3%), making it unsuitable for fiber lasers where large optical absorption and modulation depth are typically needed.[13] For a given optical absorption, high modulation depth can be typically achieved by minimizing the non-saturable losses (the optical loss of SAs at high irradiation intensity).[44] For SWNT-based SAs, nanotube bundles and aggregations mostly contribute to these. The most widely employed approach to avoid excessive non-saturable losses is de-bundling the SWNTs *via* solution processing techniques and embedding them into polymer matrices.[42] Indeed, this strategy, coupled with matching the SWNT absorption peak with the operation wavelength, is followed in the majority of the SWNT-based photonic devices,[15, 36, 42] giving a typical non-saturable loss of ~50% of total linear absorption.[15, 42] However, when using a wide range of tube diameters to achieve a 'broad-band' SWNT SA, the high loading of SWNTs required in the devices result in instability of nanotube dispersion during the composite preparation, leading to aggregation and therefore, high non-saturable absorption losses and small modulation depth.

Good SAs should also have a low value of saturation intensity,[45] I_{sat}. This is defined as the optical intensity required to reduce the SA absorption coefficient to half of the initial value, considering zero non-saturable absorption losses.[44] In graphene, I_{sat} is estimated to be in the range of a few tens[30, 46, 47] of MW/cm^2. For SWNTs, I_{sat} is in the range of ~30GW/cm^2 in aqueous dispersions.[48] For multiwall nanotubes (MWNTs) with ~40nm outer diameter, I_{sat} is >100GW/cm^2 in aqueous dispersions.[49, 50] Therefore, when compared with SWNTs and graphene, MWNTs require higher irradiation intensity to reach absorption saturation.[49, 50] This is why except for only a handful of reports,[51] MWNTs have not been traditionally considered as SAs for passive mode-locking.

The concentric tube arrangement makes DWNTs an interesting class of nanomaterials, with a wide-ranging potential applications, including in (opto)electronics.[52-54] Of particular interest relevant to this work, DWNTs also exhibit ultrafast carrier dynamics.[48, 55-57] Ref. [48] measured a linear limit of saturable

absorption (α_0 ~6.1 x 10^3 and ~6.4 x 10^3 cm^{-1}) and I_{sat} (~68 and 14GW/cm^2) for aqueous dispersions and thin-films of DWNTs, respectively. This is similar to the values reported for SWNT aqueous dispersions by the same authors (α_0 ~5.6 x 10^4 cm^{-1} and I_{sat}~33GW/cm^2, respectively).[48] Thus, in terms of carrier dynamics, DWNTs are comparable to SWNTs.

Further, DWNTs can have outer and inner wall combinations with different electronic types (semiconducting, *s* or metallic, *m*) in their structures (outer-inner: *s-s*, *s-m*, *m-s* and *m-m*), resulting in different charge transfer behaviors between the tubes.[58] With semiconducting outer tube for *s-s* and *s-m* combinations, optical absorption from excitonic transition energies of both the inner and outer walls are expected to contribute to the overall optical absorption of the resultant DWNT structure, making them suitable as wideband SAs. Conversely, with metallic outer wall for the *m-s* and *m-m* combinations, the outer wall has zero band gap with wide absorption range and may create a screening effect,[59] suppressing optical absorption from the inner *s*- or *m*-nanotubes. Nevertheless, such combination may also work as an advantage for ultrafast photonic applications of DWNTs. This is because the presence of inner or outer *m*-nanotubes (*s-m*, *m-s*) in the same structure can increase the carrier relaxation speed of the *s*-nanotubes as electrons and holes can tunnel from them to their metallic counterparts.[60, 61] Indeed, experimental observations indicate that the relaxation times of inner nanotubes of DWNTs are comparable or shorter[60, 62, 63] than the SWNTs of same species. For example, ref. [57] showed that under the same experimental conditions, the exciton decay time for (7,6) inner tubes in DWNTs is 0.65ps, compared to 3.2ps for a (7,6) SWNT species due to shorter exciton decay time and energy relaxation from inner to outer tubes[57] *via* exciton energy transfer (EET).[64, 65]

The strong third-order optical nonlinearity, ultrafast carrier dynamics[48, 55-57, 63] and wide optical absorption[57, 66] make DWNTs with ~1.6-1.8nm outer diameter very attractive for ultrafast photonic applications in the 1 to 2μm range. Considering an inter-wall distance of ~0.36-0.38nm,[67, 68] the diameter difference between inner and outer tubes is ~0.7-0.8nm. Therefore, DWNTs with 0.8-1.1nm inner diameter have outer tubes with 1.6-1.8nm diameter with two distinct and strong eh_{22} and eh_{11} *s*-tube

absorption bands at ~1.1 and ~2.0μm,[69] respectively. The eh_{11} from inner *s*-tubes at ~0.8-1.1μm are expected to be overlapped by eh_{22} of the outer tubes.[66,69] This makes DWNTs efficient SAs at ~1, ~2μm and for larger diameter tubes, potentially beyond this range. This is very attractive for bio-applications where significant demand exists for portable, tunable, pulsed laser sources from ~2 to up to 10μm.[70] Similar to other nanoparticles, the aggregation phenomenon of nanotubes, especially in low viscosity dispersions, is largely governed by diffusion process of nanotubes and nanotube-nanotube interactions in a certain medium.[71] This is in addition to the effect of solvent properties (*e.g.,* pH) and stabilization by dispersant (*e.g.,* surfactants). In low viscosity dispersions, aggregation between nanotubes can therefore increase significantly with increased nanotube concentration because of more 'exposed' nanotube surfaces.[72] The processing technique we use here involves slow evaporation of solvents from a low viscosity (1.6mPa.s at 25ºC) mixture. This highlights the need for a stable dispersion to avoid large aggregation during solvent evaporation. DWNTs allow two nanotubes in a single structure, minimizing the possibility of such large (>1μm) aggregations and bundle formation during composite fabrication, and thus scattering losses while potentially offering high modulation depth at a range of wavelengths. Here, we demonstrate DWNT-polymer composites as broadband passive mode-lockers for ultrafast pulse generation at 1, 1.5 and 2μm in Yb-, Er- and Tm- doped fiber laser cavities, respectively.

RESULTS AND DISCUSSION

We use DWNTs produced by Catalytic Chemical Vapor Deposition (CCVD) of CH_4 over $Mg_{1-x}Co_xO$ solid solution containing Mo oxide.[73] After CCVD, the nanotubes are oxidized in air at 570°C for 30min.[74] The residual material is next washed with HCl to dissolve the metal oxides.[74] Figures 1(a-c) are representative TEM images of the DWNT samples at different magnifications. Statistics on ~130 DWNTs reveals that they have ~1.1nm inner and ~1.8nm outer mean diameters, Figs. 1(d,e). TEM images of ~145 tubes also indicate that the purified samples contain ~90% DWNTs, ~8% SWNTs and ~2% TWNTs.

Optical absorption and photoluminescence excitation (PLE) spectroscopy of this purified nanotube sample dispersed with sodium dodecylbenzene sulfonate (SDBS) surfactant in deuterium oxide (D_2O) is

then used to characterize the DWNT samples. Using D_2O instead of water allows extension of the spectral study region of the dispersions in the NIR. Pure water begins to absorb at ~700nm, followed by a series of strong absorption peaks above ~900nm, with complete absorption just above 1100nm. Using D_2O instead of H_2O means O–H is substituted by O–D, pushing all these water related absorption peaks by $\sim\sqrt{2}$ times towards the higher wavelength, *i.e.,* to beyond ~1300nm and ~1800nm for the case of the strong peaks and complete absorption, respectively.

Figure 2 plots the absorption spectrum of the purified nanotubes dispersed in D_2O. The peak at ~1.1μm corresponds to eh_{11} excitonic transitions of 0.75-1.15nm inner tubes, overlapping with the eh_{22} of 1.5-1.9nm outer tubes.[66, 69] The reference spectrum of D_2O is also presented, highlighting that the eh_{22} absorption peaks of the outer wall of DWNTs cannot be resolved above 1800nm due to strong optical absorption from D_2O.

Figure 3 plots the photoluminescence excitation (PLE) map of the purified nanotube sample (~90% DWNTs, ~8% SWNTs and ~2% TWNTs). The chiralities are assigned according to ref. [69]. The PLE map shows strong emissions from the diameter range of ~0.7-1.15nm. This corresponds to that of the inner tubes as derived by TEM, Fig. 1(e). Ref. [64, 65] reported ~2-3mev red-shift in eh_{11} and eh_{22} of small SWNT bundles, which formed with two months of aggregation after they were dispersed in water-SDBS solution. Here, we observe a ~5-7meV red-shift in eh_{11} and eh_{22} of all the nanotube species compared to the aforementioned aggregated SWNTs. We attribute such red spectral shifts, even larger than those of the aggregated nanotubes,[64, 65] to the dielectric screening[75] of the inner tubes by the outer tubes in DWNTs.[62] Such large redshift could also be due to bundle formation of the individual *s*-SWNTs (*i.e.,* not the inner tubes in DWNTs, but a % of the 8% SWNTs) present in the sample. However, we do not observe significant evidence of bundle formation through strong optical signatures of exciton energy transfer (EET) between *s*-nanotubes of similar diameter. In line with our TEM observation, this indicates that the population of individual *s*-SWNTs present in the sample is very low. We argue that the (eh_{22},eh_{11}) emission from small tubes comes from the inner *s*-nanotubes of DWNTs which, despite bundling of the

DWNTs, have weak EET due to larger physical spacing between themselves (>0.7nm as opposed to ~0.34nm in standard SWNT bundles discussed in ref. [64, 65, 76]). This is because the EET process between *s*-nanotubes in small bundles occurs *via* Förster Resonance Energy Transfer (FRET), whose efficiency is dependent on the inverse 6th power of the physical distance between the donor acceptor couple.[77] Note that our observation and explanation supports PL from inner tubes as observed by ref. [62, 78, 79] but contrasts reports that the PL emission from the inner tubes in DWNTs are strongly quenched[80] by the outer tubes by up to four orders of magnitude.[81] We only detect very weak or no emissions above 1375nm range, from tubes with d_t ~1.2-1.3nm. Indeed, tubes at this d_t range constitute only a very small % of the overall population, as evident from the TEM (Fig. 1(e,f)) and absorption spectra of nanotubes in the dispersion (Fig. 2). As discussed later, the nanotube-polymer composite (Fig. 6) also shows weak absorption (from eh_{11} excitonic transitions) in the 1400-1600nm range *i.e.*, for d_t ~1.2-1.3nm. The outer tubes of the DWNTs with a mean d_t ~1.8nm, are expected to emit in the ~1800-2000nm range from their eh_{11} excitonic transitions and cannot be measured from their dispersed state in D_2O because of strong optical absorption of D_2O in this range (Fig. 2).

Raman spectra of the purified nanotube powder are measured at 457nm (2.71eV), 488nm (2.54eV), 514.5nm (2.41eV), 632.8nm (1.96eV) and 785nm (1.58eV) to further characterize the nanotubes. In the low frequency region, the Radial Breathing Modes (RBMs) are observed. Their position Pos(RBM), is inversely related to SWNT diameter, d_t[82-84] as given by $\text{Pos(RBM)}=C_1/d_t + C_2$. Combining Pos(RBM), with excitation wavelength and '*Kataura plot*'[69, 85] it is, in principle, possible to derive the SWNT chirality.[86, 87] A variety of C_1 and C_2 were proposed for this relation.[83, 84, 87, 88] Here, we use C_1=228.8 cm^{-1} and C_2=2.4 cm^{-1} from ref. [89], derived by plotting the experimental Pos(RBM) to d_t relationship for CVD grown DWNTs. However, if one is interested in estimation of the bandgap, the precise choice of constants is less critical, as the difference in the calculated diameter from the actual value is small. The typical Raman spectrum of nanotubes in the 1500-1600cm^{-1} region consists of the G^+ and G^- bands. In *s*-SWNTs, they originate from the longitudinal (LO) and tangential (TO) modes, respectively, derived from the splitting of the E_{2g} phonon of graphene.[90-92] The positions of the G^+ and G^- peaks, Pos(G^+), Pos(G^-), are

diameter dependent and the separation between them increases with decreasing diameter.[91] In *m*-SWNTs, a wide, low frequency G^- is a fingerprint of *m*-SWNTs. On the other hand, the absence of such feature does not necessarily imply that only *s*-SWNTs are present, but could just signify that *m*-SWNTs are off-resonance.

Thus, a large number of excitation wavelengths are necessary for a complete characterization of nanotubes.[82, 88] In particular, we note that ref. [93] reported that tubes with up to 100meV off resonance from the excitation wavelength can be detected. It is important to note that tubes in resonance with the same laser energy can also have a different diameter.

Figure 4(a) plots RBM region for the nanotube samples. Note that the RBM detection range is limited by the cutoff of the notch and edge filters at 140, 160, 150, 130 and 150cm^{-1} for 457nm, 488nm, 514.5nm, 632.8nm, and 785nm, respectively. Thus, we can detect tubes with diameter up to 1.8nm at 632.8nm, while we cannot detect tubes with diameter >1.45nm at 488nm. For each excitation wavelength, we use Lorentzians to fit the RBMs from 20 different measurements to derive the statistics presented in Figs. 5(a-e). The RBM spectra do not reveal a cluster distribution of inner and outer peaks around two well-defined diameters. Rather, they show a broad distribution, spanning the entire range from 140cm^{-1} to 400cm^{-1}. This heterogeneous distribution was also observed in other Raman characterization of CVD grown DWNTs.[89, 94] The counts in Figs. 5(a-e) represent how many times the nanotubes of a particular diameter were observed due to resonance with the excitation wavelength. Keeping this in mind, the RBM results are in agreement with optical absorption and PLE measurements.

Figures 4(b), (c) plot the Raman spectra in the *G* and *2D* region obtained from the nanotube powders, respectively. Very weak *D* band contributions are also observed in the *G* region, indicating a small number of defects.[95, 96] The G^+ and G^- peaks are fitted with Lorentzians. The diameter dependence of G^+ and G^- peaks can be used to determine the diameter distribution of the nanotubes.[91] This gives an outer tube diameter range of 1.4-1.8nm. On the other hand, inner tubes have a diameter distribution in the 0.6-1.0nm range. The estimation for the inner tubes agrees well with the results of RBMs and the *G* region.

For the case of the outer tubes, we cannot compare with the RBM data due to the cutoff of notch/edge filter. However, the data agrees with the Raman analysis of the *G* band and TEM, where a distribution of ~1.7nm is estimated for the outer tubes. The 2D bands in Figure 4(c), under different excitations, show a spectral profile with multiple Lorentzian peaks, similar to other reports on DWNTs.[97] Therefore, we expect strong absorption bands at ~1.1 and ~2μm from this nanotube sample. This enables us to maximize the change in absorption under strong optical irradiation,[15] making them ideal SA materials at these wavelengths.

We use the purified nanotubes to prepare nanotube-polymer composites to take the fabrication and integration advantage of polymer photonics into various lightwave systems[15] as well as the optical properties of the constituent ~90% DWNTs. First, the nanotube sample is ultrasonically dispersed in water using sodium dodecylbenzene sulfonate (SDBS) surfactant, centrifuged to remove the large insoluble particles, mixed with aqueous polyvinyl alcohol (PVA) solution and sonicated again to obtain a homogeneous and stable dispersion free of aggregations. We use water as the solvent and SDBS as the surfactant to obtain higher concentration of isolated nanotubes or small bundles[98] than possible with non-aqueous solvents.[99-101] PVA is used for its solvent compatibility. Slow evaporation of water at room temperature produces a freestanding, ~50μm thick nanotube-PVA composite (~90% DWNTs, 8% SWNTs and 2% TWNTs).

Figure 6 shows the optical absorption of the nanotube-polymer composite. This has two absorption bands centered at ~1.1 and ~2μm with a peak width of ~250 and ~350nm, respectively. This corresponds to distinct diameter range d_t~0.75-1.15nm (eh_{11} at ~1.1μm) and ~1.5-1.9nm (eh_{11} at ~2μm and eh_{22} at ~1.1μm),[69] respectively. This matches the inner and outer diameter distributions of the DWNTs. The 8% SWNTs present in the sample have a diameter range similar to that of the inner wall of DWNTs. Thus, eh_{11} absorption of these SWNTs also contribute to the strong ~1.1μm absorption peak from the eh_{11} of inner and eh_{22} of the outer walls of DWNTs. The inner walls of the 2% TWNTs have diameter ~2nm as observed by TEM. We do not observe any significant eh_{11} or eh_{22} absorption peaks from the inner walls of

the TWNTs. Note that although the eh_{22} excitonic transitions of *s*-SWNTs can extend the operation range of SWNTs to shorter wavelengths,[102] the $eh_{22} \rightarrow eh_{11}$ relaxation is over one-order of magnitude smaller than $eh_{11} \rightarrow$ ground state relaxation.[103] This increases the I_{sat} at eh_{22} transition by over one of magnitude compared to that at eh_{11} transition, making the SA device difficult to saturate at the wavelengths corresponding to eh_{22}.[102] We argue that the presence of inner walls in DWNTs and strong contribution from their eh_{11} transition at 1.1μm contribution ensures I_{sat} comparable to that of the SWNTs. Similarly, MWNTs, as discussed before, also have high saturation intensity,[49, 50] which limits their SA applicability.

Small aggregation of CNTs (<1μm), in general, is considered beneficial for saturable absorption. Indeed, such level of bundling improves carrier relaxation times by up to an order of magnitude[104] by providing multiple relaxation pathways for the excited carriers.[105] However, these bundles/aggregates are beyond the standard optical microscope resolution limit. Thus, typical optical microscopy is usually used to identify samples with large (>1μm) aggregates, which are more likely to exhibit large scattering (*i.e.*, non-saturable) losses.[15] Optical microscopy (Figure 6, Inset) reveals no large nanotube aggregations or defects in the composite, thus avoiding such losses.[106]

The polymeric film-based device is integrated by taking a ~2mm^2 nanotube-polymer composite, sandwiching it between a fiber pigtailed fiber connector with physical contact (FC/PC) with index matching gel at both the fiber ends. The index matching gel is used to reduce the insertion losses. The SA device is used to demonstrate mode-locking at 1, 1.5 and ~2.0μm. The fundamental working principle for the nanotube-based SA devices is explained in refs. [15, 42]

Figure 7(a) shows the setup for 1μm. A 2m Yb-doped fiber-based optical amplifier is used to provide gain for lasing. This is a commercial IPG amplifier unit with 25dB gain at the signal wavelength. A polarization controller is employed for mode-locking optimization. A fused 20/80 coupler is utilized as the output coupler. The 20% port is used for the measurements. All of the cavity fiber has positive group-velocity dispersion (GVD) ($\beta_2 \approx 18$ ps^2 km^{-1}). A circulator and chirped fibre Bragg grating (CBG) are inserted inside the ring cavity to set the overall GVD negative, to facilitate soliton-like pulse shaping

through the interplay of group velocity dispersion and self-phase modulation[109]. The total cavity length is ~12.5m.

Stable mode-locking at 1μm is achieved. No pulses are observed after removing the composite from the cavity, confirming mode-locking is initiated by the DWNT composite. Figure 7(b) plots a typical second harmonic generation autocorrelation trace, which is well fitted by a $sech^2$ temporal profile. This gives a full-width at half-maximum (FWHM) pulse duration of 4.85ps. Such broad pulse is mainly caused by large overall negative GVD.[109] The output spectral data is shown in Fig. 7(c). The output spectrum peaks at 1066nm with FWHM=0.284nm. The sidebands are typical of soliton operation, due to intracavity periodical perturbations,[108] the asymmetry can be attributed to the significant third-order dispersion introduced by the chirped fiber Bragg grating.[108, 109] The time-bandwidth product (TBP) of the output pulses is 0.36. The deviation from TBP=0.31 expected for transform-limited $sech^2$ pulses[109] indicates the presence of minor chirping of the output pulses[109]. The output repetition rate is ~16.37MHz. Typical output power is 0.12mW, with single pulse energy of 7.3pJ. These results are comparable to those obtained with SWNTs at 1μm.[23, 24]

For 1.5μm operation, we use an erbium-doped fiber (EDF) as the gain medium, pumped by a 980nm diode laser *via* a wavelength division multiplexer (WDM). An isolator is employed after the gain fiber to ensure unidirectional operation. A polarization controller (PC) is used for mode-locking optimization. The 20% tap of the 20/80 coupler is used as output for measurement. The setup is presented in Fig. 8(a). The length of EDF is 0.8m. The gain fibre has a ~6/125μm core/cladding geometry and has an absorption of ~40dB/m at a wavelength of 1531nm. The total cavity length is 7.3m. The output pulse duration is around 532fs, assuming $sech^2$ pulse profile; see Fig. 8(b). The TBP of the output pulses at 1.5μm is 0.42. The deviation from TBP=0.31 is due to the minor chirping of the output pulses. In this case, the peak lasing wavelength is 1559nm, with FWHM=6.5nm (Fig. 8(c)). Typical soliton sidebands are also observed. The sideband intensity difference is mainly because of higher EDF gain at ~1545nm compared to that at ~1570nm.[107, 108]

For ~2.0μm operation, we construct a ring laser cavity using a 3.5m-long Tm-doped silica fiber as the gain medium. The gain fibre is a single clad thulium-doped fiber from Nufern. It has a 9μm/125μm core/cladding geometry and has an absorption of ~10dB/m at a wavelength of 1560nm. An amplified 1560nm diode laser through a WDM pumps the gain fiber. A coupler is used to couple 50% light back into the cavity while guiding 50% of the incident power to the output port of the laser. The mode-locker device is on one end, connected to the wideband coupler and on the other end, spliced to an isolator to ensure unidirectional light propagation (Fig. 9(a)). A dichroic mirror is used to eliminate the residual pump power at 1560nm. At ~350mW pump power, we achieve an output power of ~1.2mW. The autocorrelation trace is shown in Fig. 9(b), which closely follows a $sech^2$ shape. The mode-locked optical spectrum in Fig. 9(c) exhibits a center wavelength of 1883nm with a FWHM spectral width of ~3.2nm. Typical sidebands are due to periodic perturbations from cavity components. The corresponding TBP is ~0.44, which again indicates the presence of chirping. The repetition rate for the output pulse train is 17.82MHz, as determined by the cavity length of ~10.8m.

Radio frequency (rf) spectrum measurements can be used to monitor the mode-locking stability[110]. The typical rf spectra at 1, 1.5 and 2μm have a peak at an output repetition rate corresponding to the cavity round trip time. This confirms reliable continuous-wave mode-locking.[111] For the rf spectrum at 1066, 1559 and 1883nm, the peak to pedestal extinction ratios are ~60, 86 and 77 dB, respectively (>10^6 contrast). This confirms a stable output pulse.[111]

CONCLUSIONS

Our demonstration of wideband mode-locking optical pulses at 1, 1.5 and 2μm using DWNT-polymer composites shows that they could potentially be useful for wideband ultrafast photonic applications. In particular, building on our experiments, Few Wall (*e.g.*, <5) Nanotubes (FWNTs) with broader absorption profile and I_{sat} lower than large diameter FWNTs may become very attractive for broadband mid-infrared applications.

EXPERIMENTAL METHODS

Transmission Electron Microscopy: For Transmission Electron Microscopy (TEM) analysis, dispersions are drop cast onto a lacey carbon support grid (400mesh). Water is readily removed by an absorbent underneath, leaving DWNTs on the carbon grid. TEM images are taken using a JEM-3000F FEGTEM at 300kV.

Raman and optical absorption spectroscopy: Raman spectroscopy measurements are carried out using a Renishaw inVia spectrometer using a 50X objective. A Perkin-Elmer Lambda 950 spectrophotometer is used for the vis-NIR absorption measurements with 1nm step.

Preparation of DWNT dispersions for photoluminescence excitation spectroscopy: 0.01wt% of purified DWNTs is ultrasonicated with 0.2wt% of SDBS in 10ml deuterium oxide (D_2O) inside a sealed glass test tube in a bath sonicator (Bioruptor; Diagenode) at 270W, 20 kHz for 4 hours. The homogeneous dispersion is then centrifuged in a TH-641 rotor using a sorvall WX 100 ultracentrifuge at ~200,000*g* for 2 hours and the top 30% decanted for PLE characterization.

Photoluminescence excitation spectroscopy: The PLE maps are taken from nanotube dispersions in a HORIBA Jobin Yvon excitation-emission spectrofluorometer (Fluorolog-3) equipped with a xenon lamp excitation source and a liquid nitrogen cooled InGaAs detector (Symphony solo). The PLE maps are measured at right angle scattering by scanning the excitation wavelength from 300nm to 900 nm with 5nm steps and 60s exposure for ~850nm to ~1450nm emission range. The entrance and exit slit widths are 14nm and 30nm, respectively.

Preparation of DWNT-PVA composites: 0.04wt% of purified DWNTs grown by CCVD method[71] is ultrasonicated in 10ml of DI water with 1wt% of SDBS using a tip sonicator (Branson 450A, 20kHz) at ~100W output power and 10ºC temperature for 4 hours. The homogeneous dispersion is centrifuged at ~100,000*g* for 30 minutes in a TH-641 rotor using a sorvall WX100 ultracentrifuge. The top 60% of the dispersion is then decanted. 4ml of this dispersion is then mixed with a 1wt% aqueous solution of 120mg PVA and is ultrasonicated again for 30 minutes. The homogeneous mixture has a viscosity of 1.6mPa.s at 25ºC, measured using a TA instruments Discovery HR-1 rheometer. This low viscosity mixture is then

dropcast and the solvent slowly evaporated at room temperature in a desiccator, resulting in a ~50μm freestanding DWNT-PVA composite.

Characterization of mode-locked pulses: The pump and average output power are monitored by a power meter. The pulse duration and spectrum are recorded using a second harmonic generation (SHG) intensity autocorrelator and an optical spectrum analyzer, respectively. To study the operation stability, we measure the rf spectrum using a photo-detector connected to a spectrum analyzer.

ACKNOWLEDGEMENTS

We thank RCT Howe for the viscosity measurements. We acknowledge funding from EPSRC GR/S97613/01, EP/E500935/1, the ERC grant NANOPOTS, a Royal Society Brian Mercer Award for Innovation. ACF is a Royal Society Wolfson Research Merit Award holder. VN wishes to knowledge support from the European Research Council (ERC Starting Grant 2DNanoCaps) and Science Foundation Ireland, PT from Major State Basic Research Project No. G2009CB929300, China, ZS from Teknologiateollisuus TT-100, the European Union's Seventh Framework Programme (No. 631610), and Aalto University, TH from NSFC (Grant no. 61150110487), and the Royal Academy of Engineering (Graphlex).

Figure 1. (((a-c) Representative TEM images of the purified DWNTs. Inner wall (e) and outer wall (f) diameter distributions as measured from the TEM images shows a mean inner and outer diameter of 1.1

and 1.8nm, respectively.))

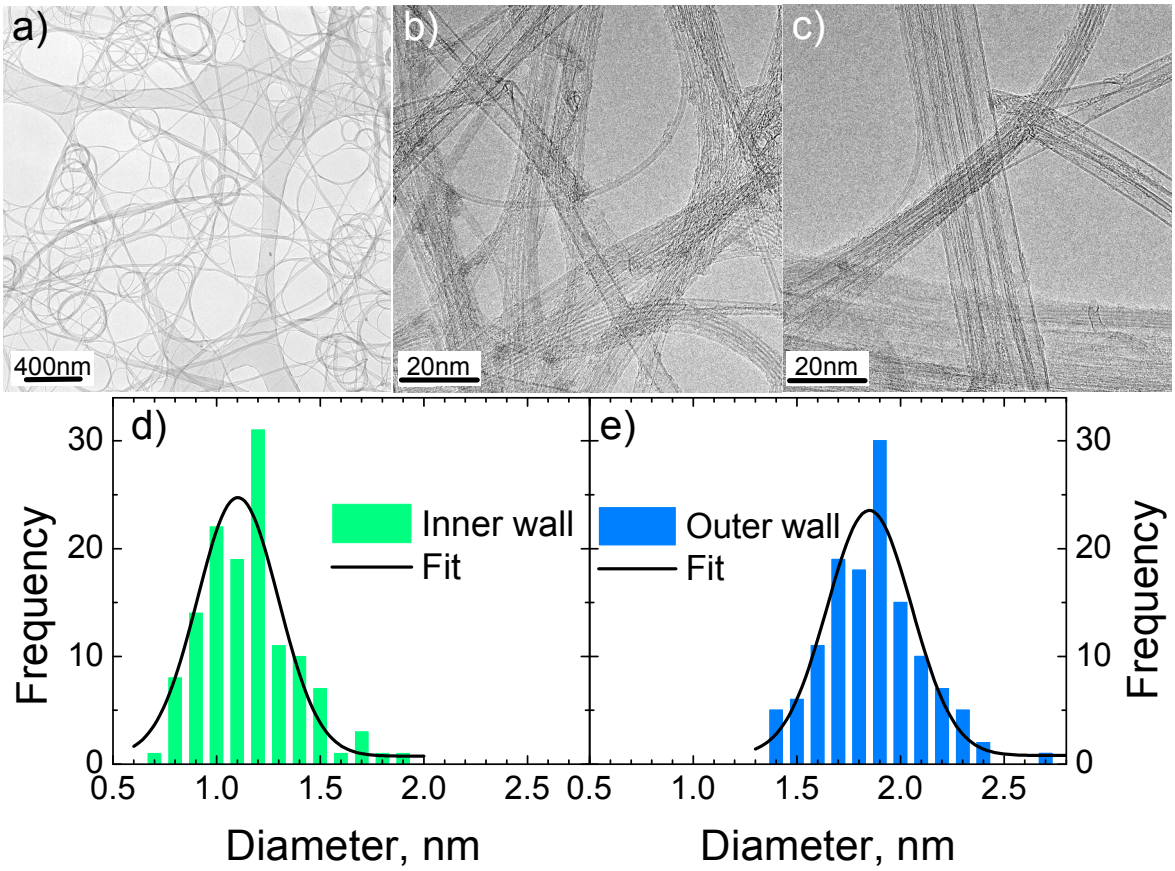

Figure 2. ((Absorption spectrum of DWNTs dispersed in D_2O in the 300-1800nm range. The contribution from D_2O is subtracted. Spectrum of D_2O is also presented.))

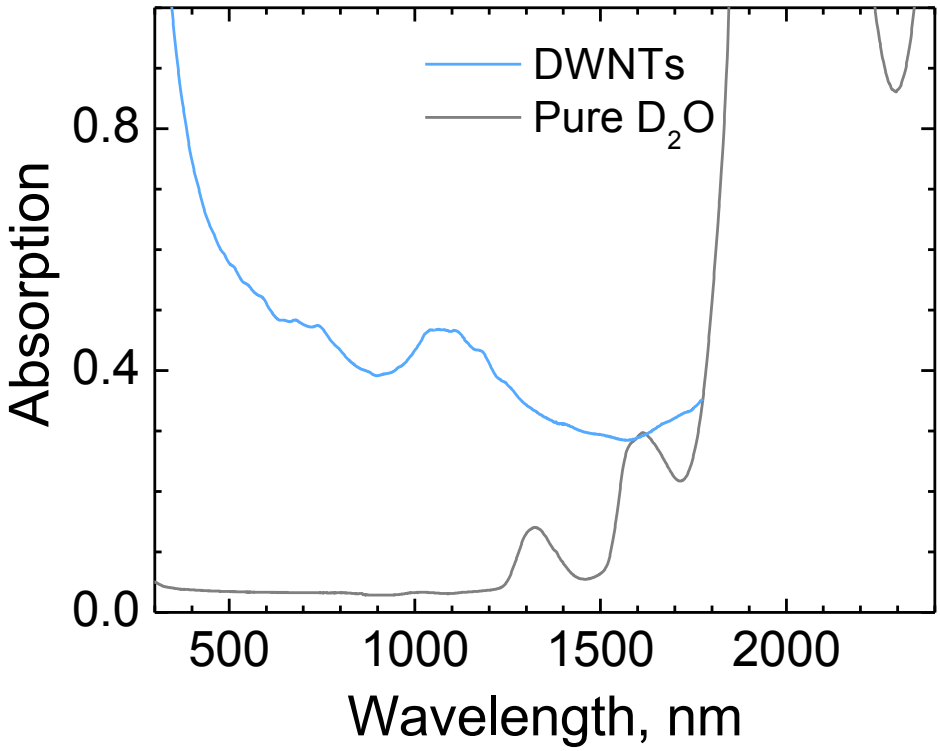
DWNTs
Pure D2O
Absorption
0.0
0.4
0.8
500
1000
1500
2000
Wavelength, nm

Figure 3. ((PLE map for DWNTs dispersed in D_2O. (n,m) is assigned following Ref.[60, 69]))

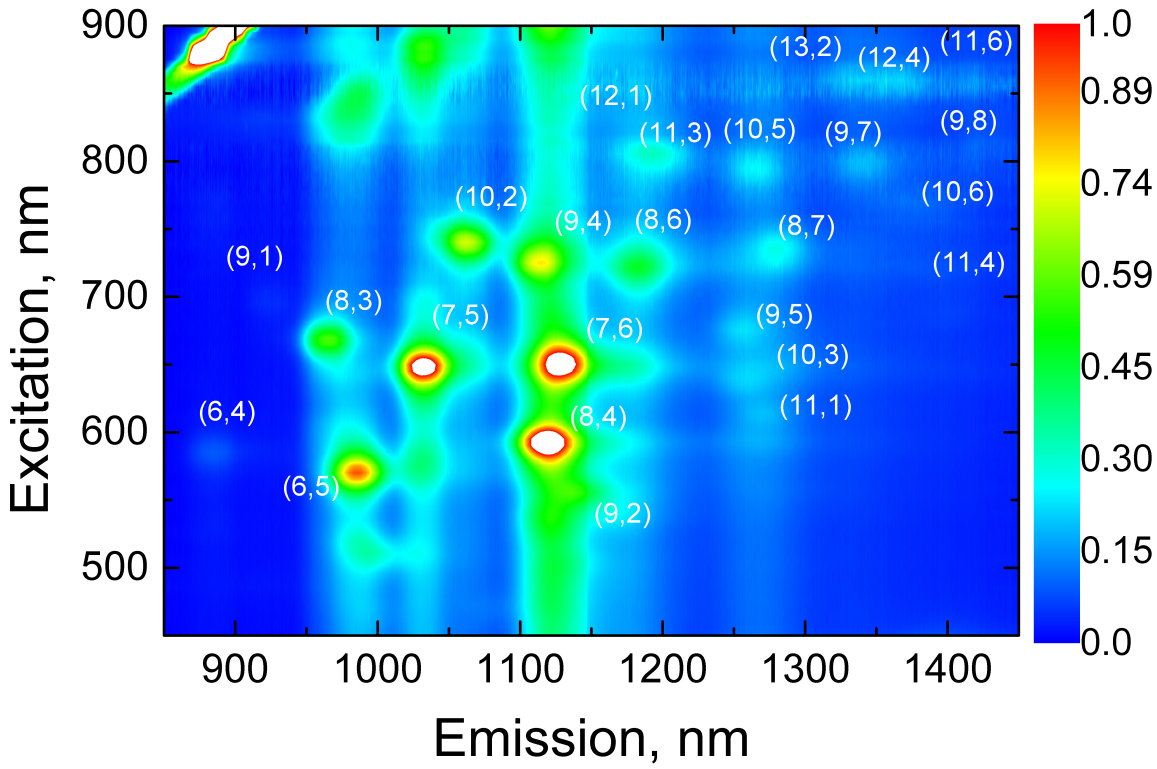

Figure 4. ((Raman spectra of DWNTs at different excitation wavelengths: a) The RBM region b) the *G* region c) the *2D* region.))

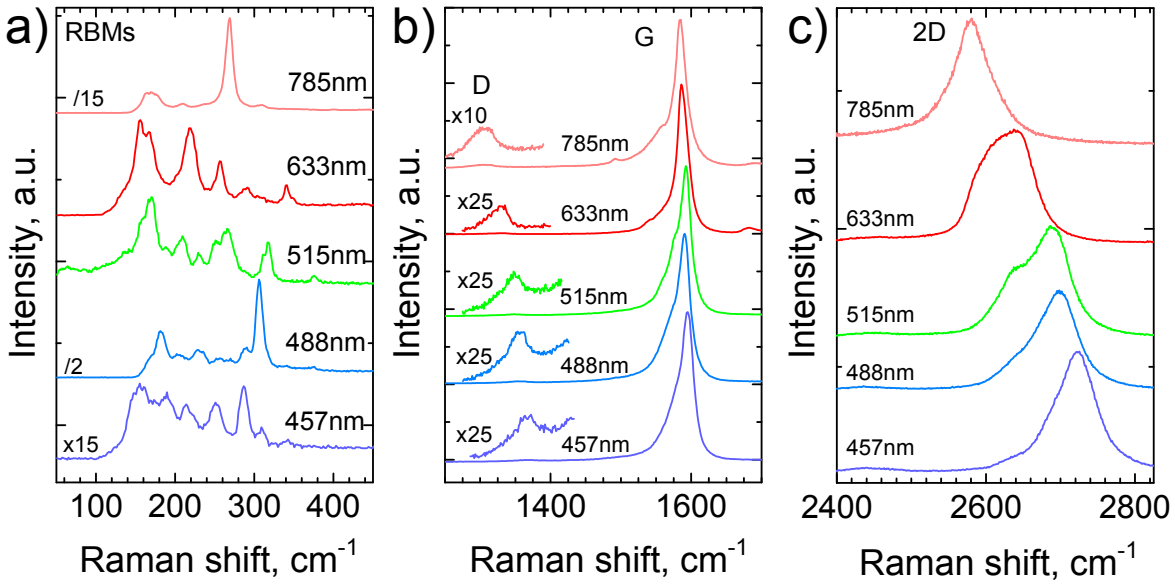

Figure 5. ((Diameter analysis from the RBMs of the nanotubes excited by 457, 488 515, 633 and 785nm wavelengths, indicating d_t ~0.6-1.8nm.))

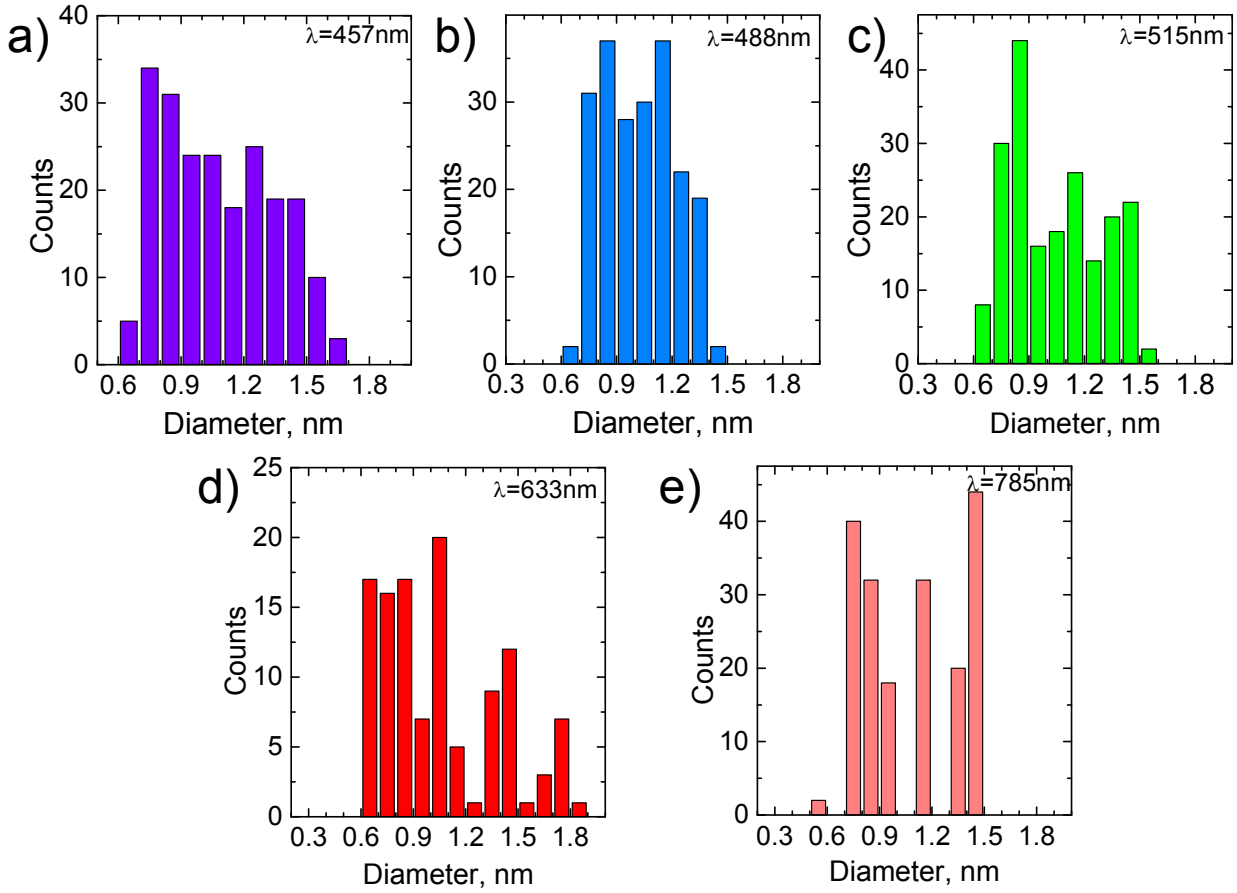

Figure 6. ((Absorption spectrum of DWNTs embedded in ~50 μm PVA polymer composite. The contribution from PVA is subtracted. Absorption spectrum of a pure PVA polymer of same thickness is also presented. Inset: Optical Microscopy of the DWNT-polymer composite reveals no nanotube aggregation.))

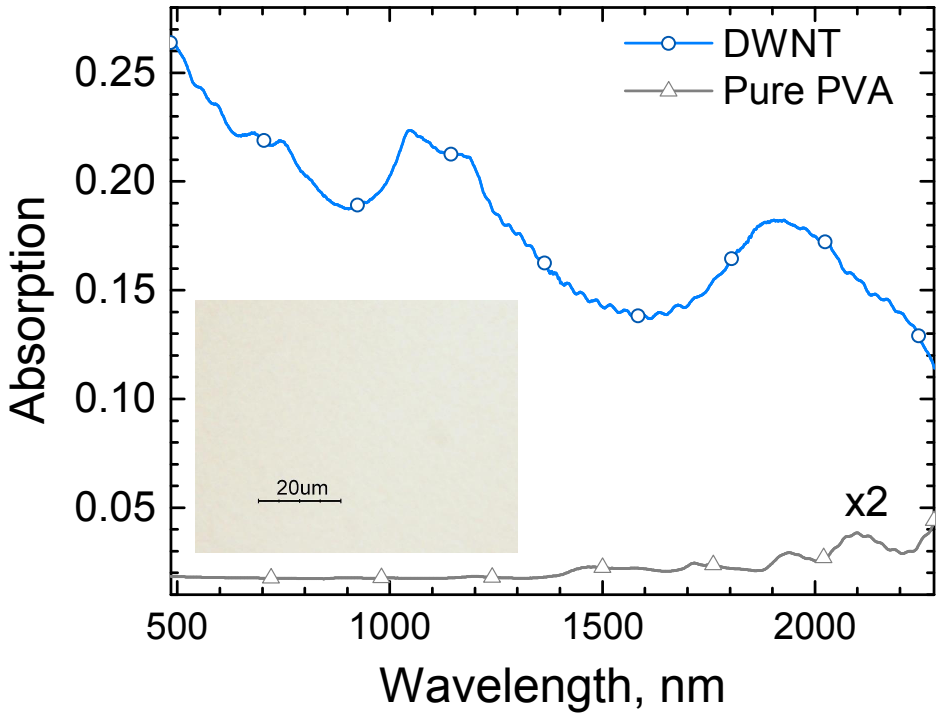

Figure 7. ((a) Laser setup at 1μm. ISO: Isolator, CBG: Chirped Bragg Grating, YDFA: Yb doped fiber amplifier, PC: Polarization Controller. The DWNT polymer composite is sandwiched between the fiber connectors. b) The second harmonic generation autocorrelation trace of the output pulses at 1μm. c) The output spectrum.))

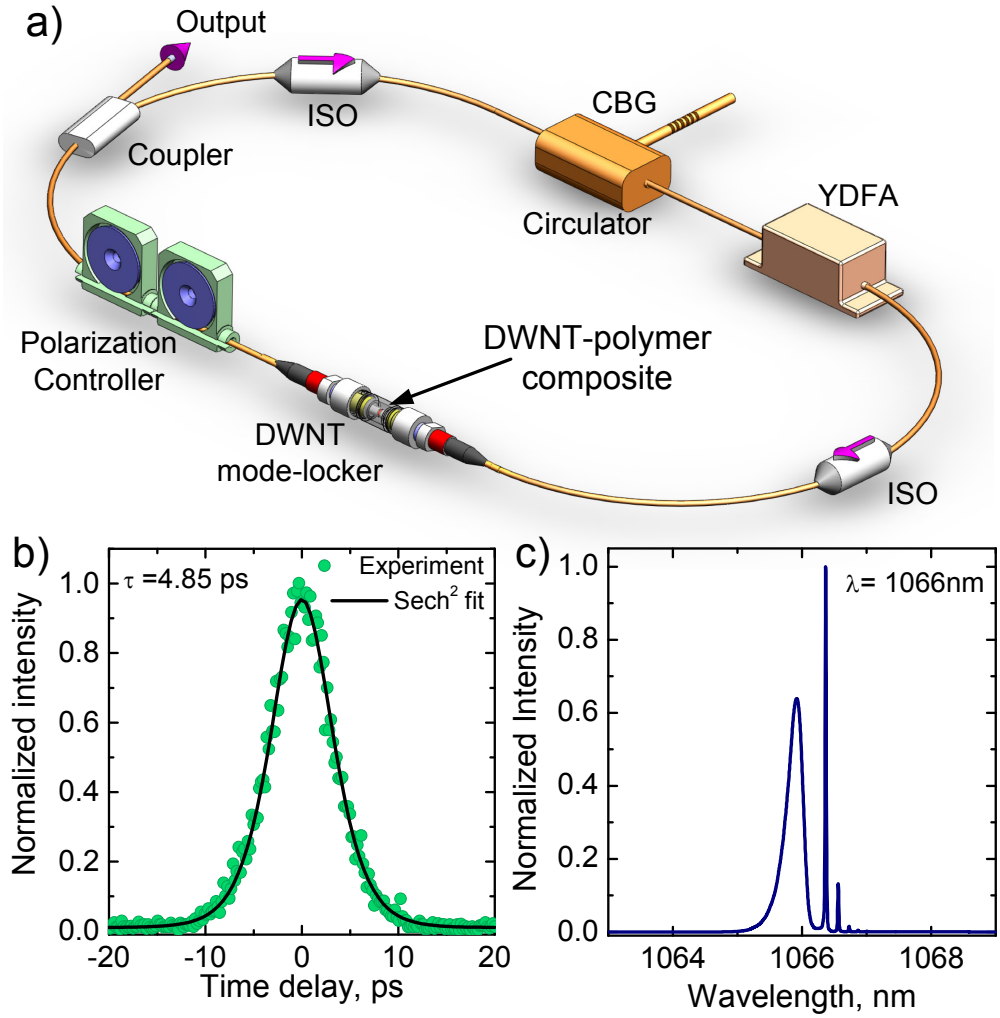

Figure 8. ((a) Laser setup at 1.5μm. EDF: Erbium doped fiber, WDM: Wavelength division multiplexer b) The second harmonic generation autocorrelation trace of mode-locked pulses at 1.5μm c) Output spectrum))

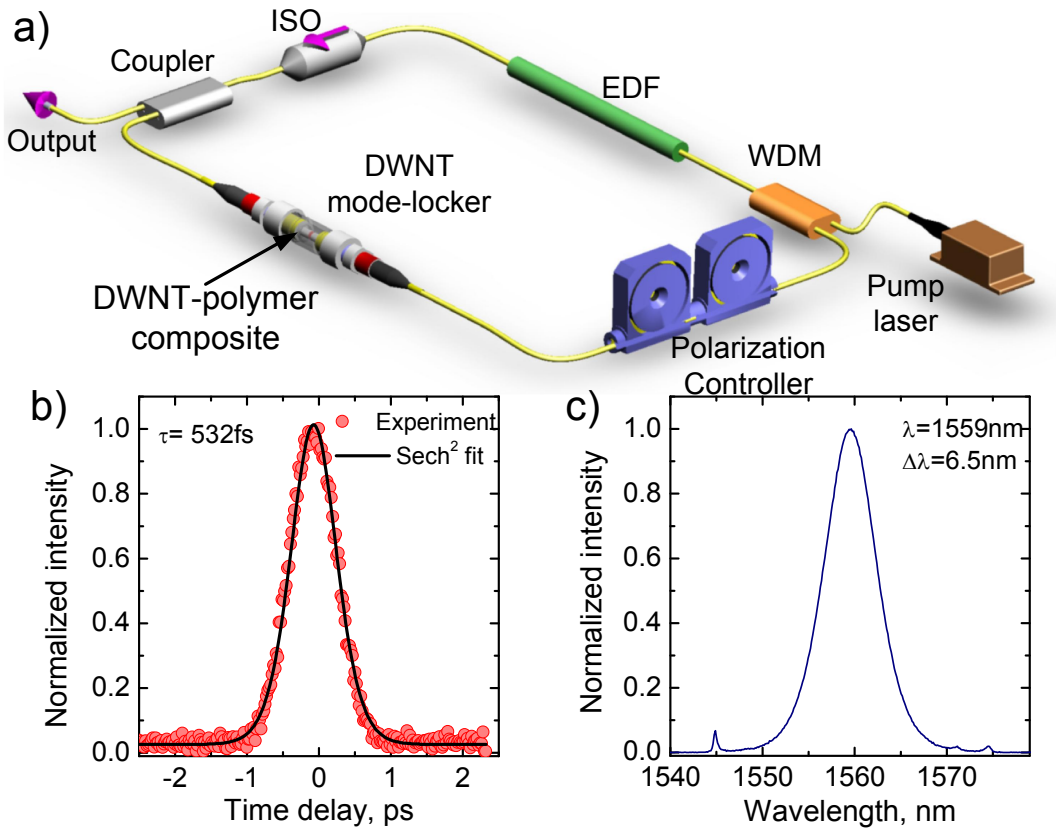

Figure 9. ((a) Laser setup at ~2μm. TDF: Thulium doped fiber b) The second harmonic generation autocorrelation trace of mode-locked pulses at ~2μm c) Output spectrum.))

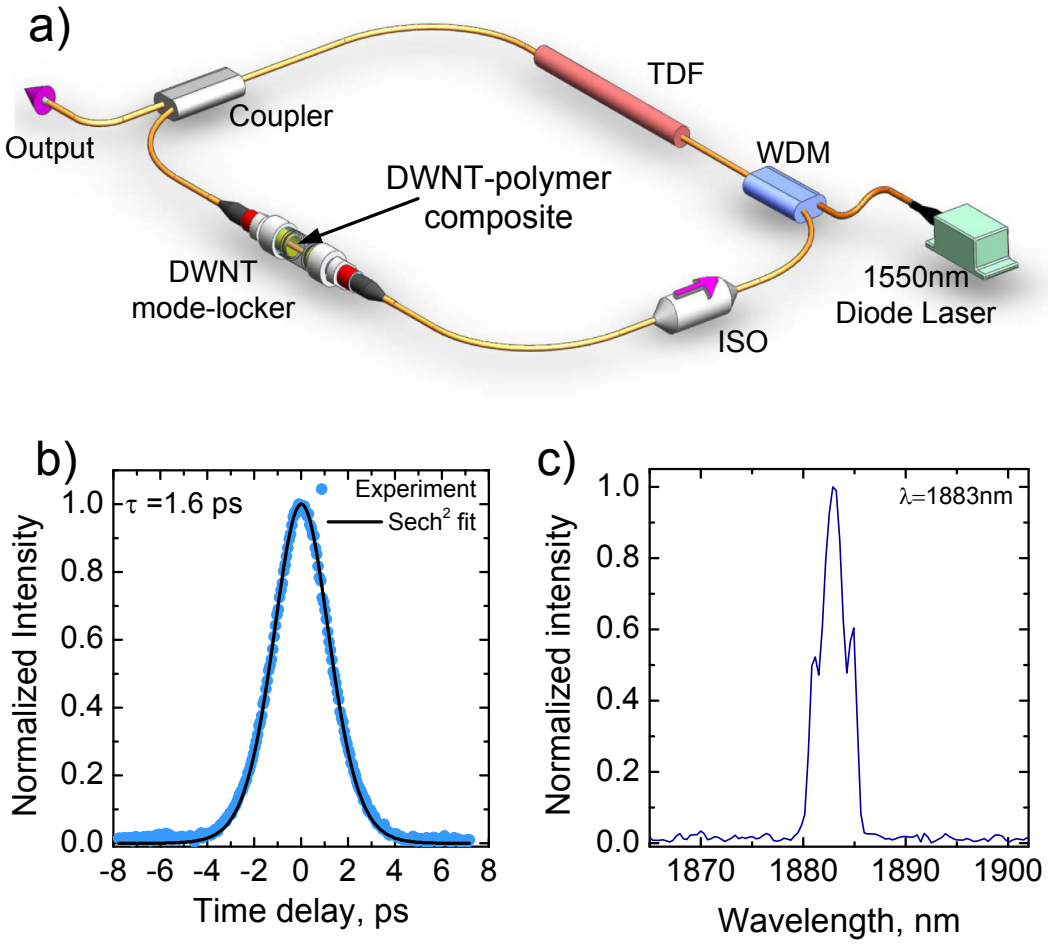

Figure 10. ((RF spectrum measured around the fundamental repetition rate a) f_1=16.37MHz, b) f_1=27.4MHz, c) f_1=17.82MHz showing peak to pedestal extinction ratios >60dB in all three wavelengths.

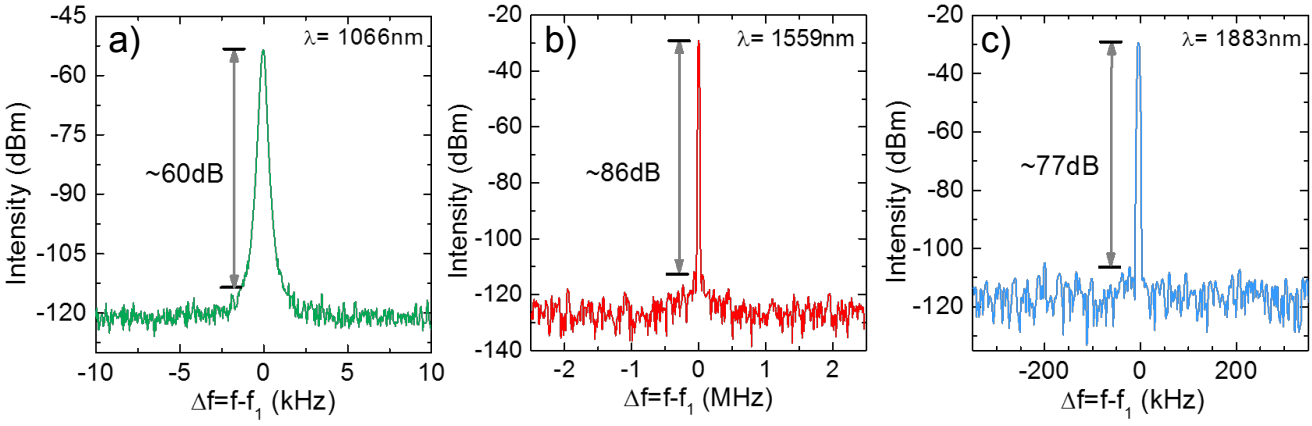

AUTHOR INFORMATION

Tawfique Hasan

Cambridge Graphene Centre, 9 JJ Thomson Avenue, Cambridge, CB3 0FA, United Kingdom.

Email: th270@cam.ac.uk

REFERENCES

[1] O'Mahony, M. J.; Politi, C.; Klonidis, D.; Nejabati, R.; Simeonidou, D. Future Optical Networks. *J. Lightwave Technol.* **2006**, *24*, 4684-4696.
[2] Leclerc, O.; Lavigne, B.; Balmefrezol, E.; Brindel, P.; Pierre, L.; Rouvillain, D.; Seguineau, F. Optical Regeneration at 40 Gb/s and Beyond. *J. Lightwave Technol.* **2003**, *21*, 2779-2790.
[3] Simon, J.; Bramerie, L.; Ginovart, F.; Roncin, V.; Gay, M.; Feve, S.; le Cren, E.; Chares, M. All-Optical Regeneration Techniques. *Annals of Telecommunications* **2003**, *58*, 1708-1724.
[4] Rouvillain, D.; Brindel, P.; Seguineau, F.; Pierre, L.; Leclerc, O.; Choumane, H.; Aubin, G.; Oudar, J. L. Optical 2R Regenerator Based on Passive Saturable Absorber for 40Gbit/s WDM Long-Haul Rransmissions. *Electron. Lett.* **2002**, *38*, 1113-1114.
[5] Hirano, A.; Kobayashi, H.; Tsuda, H.; Takahashi, R.; Asobe, M.; Sato, K.; Hagimoto, K. 10 Gbit/s RZ All-Optical Discrimination using Refined Saturable Absorber Optical Gate. *Electron. Lett.* **1998**, *34*, 198-199.
[6] Jin, C. Y.; Kojima, O.; Inoue, T.; Kita, T.; Wada, O.; Hopkinson, M.; Akahane, K. Detailed Design and Characterization of All-Optical Switches Based on InAs/GaAs Quantum Dots in a Vertical Cavity. *IEEE J. Quantum Electron.* **2010**, *46*, 1582-1589.
[7] Guina, M. D.; Vainionpaa, A. M.; Orsila, L.; Harkonen, A.; Lyytikainen, J.; Gomes, L. A.; Okhotnikov, O. G. Saturable absorber intensity modulator. *IEEE J. Quantum Electron.* **2003**, *39*, 1143-1149.
[8] Arecchi, F.; Degiorgio, V.; Sona, A. A Crossed-Beam Optical Gate With a Saturable Absorber. *Il Nuovo Cimento* **1965**, *38*, 1096-1098.
[9] Land, T. A.; Michely, T.; Behm, R. J.; Hemminger, J. C.; Comsa, G. STM Investigation of Single Layer Graphite Structures Produced on Pt(111) by Hydrocarbon Decomposition. *Surf. Sci.* **1992**, *264*, 261-270.
[10] Reid, D.; Maguire, P. J.; Barry, L. P.; Le, Q.-T.; Lobo, S.; Gay, M.; Bramerie, L.; Joindot, M.; Simon, J.-C.; Massoubre, D. *et al* All-Optical Sampling and Spectrographic Pulse Measurement using Cross-Absorption Modulation in Multiple-Quantum-Well Devices. *J. Opt. Soc. Am. B* **2008**, *25*, A133-A139.
[11] Clarke, A. M.; Anandarajah, P. M.; Bramerie, L.; Guignard, C.; Maher, R.; Massoubre, D.; Shen, A.; Oudar, J. L.; Barry, L. P.; Simon, J. C. 80-Gb/s OTDM System Analysis of a Vertical Microcavity-Based Saturable Absorber for the Enhancement of Pulse Pedestal Suppression. *IEEE Photonics Technol. Lett.* **2007**, *19*, 321-323.
[12] Keller, U. Recent Developments in Compact Ultrafast Lasers. *Nature* **2003**, *424*, 831-838.
[13] Okhotnikov, O.; Grudinin, A.; Pessa, M. Ultra-Fast Fibre Laser Systems Based on SESAM Technology: New Horizons and Applications. *New J. Phys.* **2004**, *6*, 177.
[14] Keller, U.; Tropper, A. C. Passively Modelocked Surface-Emitting Semiconductor Lasers. *Phys. Rep.* **2006**, *429*, 67-120.
[15] Hasan, T.; Sun, Z.; Wang, F.; Bonaccorso, F.; Tan, P. H.; Rozhin, A. G.; Ferrari, A. C. Nanotube-Polymer Composites for Ultrafast Photonics. *Adv. Mater.* **2009**, *21*, 3874-3899.

[16] Set, S. Y.; Yaguchi, H.; Tanaka, Y.; Jablonski, M. Ultrafast Fiber Pulsed Lasers Incorporating Carbon Nanotubes. *IEEE J. Sel. Top. Quant. Electron.* **2004**, *10*, 137-146.
[17] Sun, Z.; Rozhin, A. G.; Wang, F.; Hasan, T.; Popa, D.; O'Neill, W.; Ferrari, A. C. A compact, High Power, Ultrafast Laser Mode-Locked by Carbon Nanotubes. *Appl. Phys. Lett.* **2009**, *95*, 253102-3.
[18] Sun, Z.; Rozhin, A. G.; Wang, F.; Scardaci, V.; Milne, W. I.; White, I. H.; Hennrich, F.; Ferrari, A. C. L-band Ultrafast Fiber Laser Mode Locked by Carbon Nanotubes. *Appl. Phys. Lett.* **2008**, *93*, 061114-3.
[19] Chen, Y.-C.; Raravikar, N. R.; Schadler, L. S.; Ajayan, P. M.; Zhao, Y.-P.; Lu, T.-M.; Wang, G.-C.; Zhang, X.-C. Ultrafast Optical Switching Properties of Single-Wall Carbon Nanotube Polymer Composites at 1.55 μm. *Appl. Phys. Lett.* **2002**, *81*, 975-977.
[20] Scardaci, V.; Sun, Z.; Wang, F.; Rozhin, A. G.; Hasan, T.; Hennrich, F.; White, I. H.; Milne, W. I.; Ferrari, A. C. Carbon Nanotube-Polycarbonate Composites for Ultrafast Lasers. *Adv. Mater.* **2008**, *20*, 4040-4043.
[21] Wang, F.; Rozhin, A. G.; Scardaci, V.; Sun, Z.; Hennrich, F.; White, I. H.; Milne, W. I.; Ferrari, A. C. Wideband-Tuneable, Nanotube Mode-Locked, Fibre Laser. *Nat. Nanotechnol.* **2008**, *3*, 738-742.
[22] Beecher, S. J.; Thomson, R. R.; Psaila, N. D.; Sun, Z.; Hasan, T.; Rozhin, A. G.; Ferrari, A. C.; Kar, A. K. 320 fs Pulse Generation From an Ultrafast Laser Inscribed Waveguide Laser Mode-Locked by a Nanotube Saturable Absorber. *Appl. Phys. Lett.* **2010**, *97*, 111114-3.
[23] Kelleher, E. J. R.; Travers, J. C.; Ippen, E. P.; Sun, Z.; Ferrari, A. C.; Popov, S. V.; Taylor, J. R. Generation and Direct Measurement of Giant Chirp in a Passively Mode-Locked Laser. *Opt. Lett.* **2009**, *34*, 3526-3528.
[24] Kelleher, E. J. R.; Travers, J. C.; Sun, Z.; Rozhin, A. G.; Ferrari, A. C.; Popov, S. V.; Taylor, J. R. Nanosecond-Pulse Fiber Lasers Mode-Locked with Nanotubes. *Appl. Phys. Lett.* **2009**, *95*, 111108-3.
[25] Martinez, A.; Zhou, K.; Bennion, I.; Yamashita, S. Passive Mode-Locked Lasing by Injecting a Carbon Nanotube-Solution in the Core of an Optical Fiber. *Opt. Express* **2010**, *18*, 11008-11014.
[26] Popa, D.; Sun, Z.; Hasan, T.; Cho, W. B.; Wang, F.; Torrisi, F.; Ferrari, A. C. 74-fs Nanotube-Mode-Locked Fiber Laser. *Appl. Phys. Lett.* **2012**, *101*, 153107-4.
[27] Mary, R.; Brown, G.; Beecher, S.; Thomson, R.; Popa, D.; Sun, Z.; Torrisi, F.; Hasan, T.; Milana, S.; Bonaccorso, F. *et al* Evanescent-Wave Coupled Right Angled Buried Waveguide: Applications in Carbon Nanotube Mode-Locking. *Appl. Phys. Lett.* **2013**, *103*, 221117-5.
[28] Martinez, A.; Sun, Z. Nanotube and Graphene Saturable Absorbers For Fibre Lasers. *Nat. Photon.* **2013**, *7*, 842-845.
[29] Sun, Z.; Hasan, T.; Torrisi, F.; Popa, D.; Privitera, G.; Wang, F.; Bonaccorso, F.; Basko, D. M.; Ferrari, A. C. Graphene Mode-Locked Ultrafast Laser. *ACS Nano* **2010**, *4*, 803-810.
[30] Popa, D.; Sun, Z.; Torrisi, F.; Hasan, T.; Wang, F.; Ferrari, A. C. Sub 200 fs Pulse Generation from a Graphene Mode-Locked Fiber Laser. *Appl. Phys. Lett.* **2010**, *97*, 203106-3.
[31] Sun, Z.; Popa, D.; Hasan, T.; Torrisi, F.; Wang, F.; Kelleher, E. J. R.; Travers, J. C.; Nicolosi, V.; Ferrari, A. C. A Stable, Wideband Tunable, Near Transform-Limited, Graphene-Mode-Locked, Ultrafast Laser. *Nano Res.* **2010**, *3*, 653-660.
[32] Hasan, T.; Torrisi, F.; Sun, Z.; Popa, D.; Nicolosi, V.; Privitera, G.; Bonaccorso, F.; Ferrari, A. C. Solution-Phase Exfoliation of Graphite for Ultrafast Photonics. *Phys. Status Solidi B* **2010**, *247*, 2953-2957.
[33] Martinez, A.; Fuse, K.; Xu, B.; Yamashita, S. Optical Deposition of Graphene and Carbon Nanotubes in a Fiber Ferrule for Passive Mode-Locked Lasing. *Opt. Express* **2010**, *18*, 23054-23061.
[34] Tan, W. D.; Su, C. Y.; Knize, R. J.; Xie, G. Q.; Li, L. J.; Tang, D. Y. Mode Locking of Ceramic Nd:Yttrium Aluminum Garnet with Graphene as a Saturable Absorber. *Appl. Phys. Lett.* **2010**, *96*, 031106-3.
[35] Zhang, H.; Tang, D.; Knize, R. J.; Zhao, L.; Bao, Q.; Loh, K. P. Graphene Mode Locked, Wavelength-Tunable, Dissipative Soliton Fiber Laser. *Appl. Phys. Lett.* **2010**, *96*, 111112-3.
[36] Sun, Z.; Hasan, T.; Ferrari, A. C. Ultrafast Lasers Mode-Locked by Nanotubes and Graphene. *Physica E* **2012**, *44*, 1082-1091.

[37] Popa, D.; Sun, Z.; Hasan, T.; Torrisi, F.; Wang, F.; Ferrari, A. C. Graphene Q-Switched, Tunable Fiber Laser. *Appl. Phys. Lett.* **2011**, *98*, 073106-3.
[38] Mary, R.; Brown, G.; Beecher, S. J.; Torrisi, F.; Milana, S.; Popa, D.; Hasan, T.; Sun, Z.; Lidorikis, E.; Ohara, S. *et al* 1.5 GHz Picosecond Pulse Generation from a Monolithic Waveguide Laser with a Graphene-Film Saturable Output Coupler. *Opt. Express* **2013**, *21*, 7943-7950.
[39] Fu, B.; Hua, Y.; Xiao, X.; Zhu, H.; Sun, Z.; Yang, C. Broadband Graphene Saturable Absorber for Pulsed Fiber Lasers at 1, 1.5 and 2 μm. *IEEE J. Sel. Top. Quantum Electron.* DOI: 10.1109/JSTQE.2014.2302361 (2014).
[40] Zaugg, C. A.; Sun, Z.; Wittwer, V. J.; Popa, D.; Milana, S.; Kulmala, T. S.; Sundaram, R. S.; Mangold, M.; Sieber, O. D.; Golling, M. *et al* Ultrafast and Widely Tuneable Vertical-External-Cavity Surface-Emitting Laser, Mode-Locked by a Graphene-Integrated Distributed Bragg Reflector. *Opt. Express* **2013**, *21*, 31548-31559.
[41] Kivistö, S.; Hakulinen, T.; Kaskela, A.; Aitchison, B.; Brown, D. P.; Nasibulin, A. G.; Kauppinen, E. I.; Härkönen, A.; Okhotnikov, O. G. Carbon Nanotube Films for Ultrafast Broadband Technology. *Opt. Express* **2009**, *17*, 2358-2363.
[42] Hasan, T.; Scardaci, V.; Tan, P. H.; Bonaccorso, F.; Rozhin, A. G.; Sun, Z.; Ferrari, A. C., in *Molecular- and Nano-Tubes*, (Eds: Hayden, O., Nielsch, K.), Springer US, **2011**.
[43] Bonaccorso, F.; Sun, Z.; Hasan, T.; Ferrari, A. C. Graphene Photonics and Optoelectronics. *Nat. Photon.* **2010**, *4*, 611-622.
[44] Boyd, R. W., *Nonlinear Optics*, Academic Press, San Diego **2003**.
[45] Zitter, R. N. Saturated Optical Absorption Through Band Filling in Semiconductors. *Appl. Phys. Lett.* **1969**, *14*, 73-74.
[46] Cho, W. B.; Kim, J. W.; Lee, H. W.; Bae, S.; Hong, B. H.; Choi, S. Y.; Baek, I. H.; Kim, K.; Yeom, D.-I.; Rotermund, F. High-quality, Large-Area Monolayer Graphene for Efficient Bulk Laser Mode-Locking Near 1.25μm. *Opt. Lett.* **2011**, *36*, 4089-4091.
[47] Xing, G.; Guo, H.; Zhang, X.; Sum, T. C.; Huan, C. H. A. The Physics of Ultrafast Saturable Absorption in Graphene. *Opt. Express* **2010**, *18*, 4564-4573.
[48] Kamaraju, N.; Kumar, S.; Kim, Y. A.; Hayashi, T.; Muramatsu, H.; Endo, M.; Sood, A. K. Double Walled Carbon Nanotubes as Ultrafast Optical Switches. *Appl. Phys. Lett.* **2009**, *95*, 081106-3.
[49] Elim, H. I.; Ji, W.; Ma, G. H.; Lim, K. Y.; Sow, C. H.; Huan, C. H. A. Ultrafast Absorptive and Refractive Nonlinearities in Multiwalled Carbon Nanotube Films. *Appl. Phys. Lett.* **2004**, *85*, 1799-1801.
[50] Lim, S. H.; Elim, H. I.; Gao, X. Y.; Wee, A. T. S.; Ji, W.; Lee, J. Y.; Lin, J. Electronic and Optical Properties of Nitrogen-Doped Multiwalled Carbon Nanotubes. *Phys. Rev. B* **2006**, *73*, 045402-6.
[51] Zhang, L.; Wang, Y.; Yu, H.; Sun, L.; Hou, W.; Lin, X.; Li, J. Passive Mode-Locked Nd:YVO_4 Laser using a Multi-Walled Carbon Nanotube Saturable Absorber. *Laser Phys.* **2011**, *21*, 1382-1386.
[52] Shen, C.; Brozena, A. H.; Wang, Y. H. Double-Walled Carbon Nanotubes: Challenges and Opportunities. *Nanoscale* **2011**, *3*, 503-518.
[53] Piao, Y.; Chen, C.-F.; Green, A. A.; Kwon, H.; Hersam, M. C.; Lee, C. S.; Schatz, G. C.; Wang, Y. Optical and Electrical Properties of Inner Tubes in Outer Wall-Selectively Functionalized Double-Wall Carbon Nanotubes. *J. Phys. Chem. Lett.* **2011**, *2*, 1577-1582.
[54] Jariwala, D.; Sangwan, V. K.; Lauhon, L. J.; Marks, T. J.; Hersam, M. C. Carbon nanomaterials for electronics, optoelectronics, photovoltaics, and sensing. *Chem. Soc. Rev.* **2013**, 42, 2824-2860.
[55] Kamaraju, N.; Kumar, S.; Karthikeyan, B.; Moravsky, A.; Loutfy, R. O.; Sood, A. K. Ultrafast Electron Dynamics and Cubic Optical Nonlinearity of Freestanding Thin Film of Double Walled Carbon Nanotubes. *Appl. Phys. Lett.* **2008**, *93*, 091903-3.
[56] Nakamura, A.; Tomikawa, T.; Watanabe, M.; Hamanaka, Y.; Saito; Ago, H. Non-Linear Optical Response and Relaxation Dynamics in Double-Walled Carbon Nanotubes. *J. Lumin.* **2006**, *119-120*, 8-12.
[57] Nakamura, A.; Hikosaka, N.; Imamura, S.; Takahashi, Y.; Ago, H.; Kishida, H. Third-Order Nonlinear Optical Response in Double-Walled Carbon Nanotubes. *J. Lumin.* **2009**, *129*, 1722-1725.

[58] Kalbac, M.; Green, A. A.; Hersam, M. C.; Kavan, L. Probing Charge Transfer between Shells of Double-Walled Carbon Nanotubes Sorted by Outer-Wall Electronic Type. *Chem. Eur. J.* **2011**, *17*, 9806-9815.
[59] Chen, G.; Bandow, S.; Margine, E. R.; Nisoli, C.; Kolmogorov, A. N.; Crespi, V. H.; Gupta, R.; Sumanasekera, G. U.; Iijima, S.; Eklund, P. C. Chemically Doped Double-Walled Carbon Nanotubes: Cylindrical Molecular Capacitors. *Phys. Rev. Lett.* **2003**, *90*, 257403-4.
[60] Hertel, T.; Hagen, A.; Talalaev, V.; Arnold, K.; Hennrich, F.; Kappes, M.; Rosenthal, S.; McBride, J.; Ulbricht, H.; Flahaut, E. Spectroscopy of Single- and Double-Wall Carbon Nanotubes in Different Environments. *Nano Lett.* **2005**, *5*, 511-514.
[61] Blau, W. J.; Wang, J. Optical Materials: Variety Pays Off for Nanotubes. *Nat. Nanotechnol.* **2008**, *3*, 705-706.
[62] Hirori, H.; Matsuda, K.; Kanemitsu, Y. Exciton Energy Transfer Between the Inner and Outer Tubes in Double-Walled Carbon Nanotubes. *Phys. Rev. B* **2008**, *78*, 113409-4.
[63] Koyama, T.; Miyata, Y.; Asaka, K.; Shinohara, H.; Saito, Y.; Nakamura, A. Ultrafast Energy Transfer of One-Dimensional Excitons between Carbon Nanotubes: a Femtosecond Time-Resolved Luminescence Study. *Phys. Chem. Chem. Phys.* **2012**, *14*, 1070-1084.
[64] Tan, P. H.; Rozhin, A. G.; Hasan, T.; Hu, P.; Scardaci, V.; Milne, W. I.; Ferrari, A. C. Photoluminescence Spectroscopy of Carbon Nanotube Bundles: Evidence for Exciton Energy Transfer. *Phys. Rev. Lett.* **2007**, *99*, 137402-4.
[65] Tan, P. H.; Hasan, T.; Bonaccorso, F.; Scardaci, V.; Rozhin, A. G.; Milne, W. I.; Ferrari, A. C. Optical Properties of Nanotube Bundles by Photoluminescence Excitation and Absorption Spectroscopy. *Physica E* **2008**, *40*, 2352-2359.
[66] Iakoubovskii, K.; Minami, N.; Ueno, T.; Kazaoui, S.; Kataura, H. Optical Characterization of Double-Wall Carbon Nanotubes: Evidence for Inner Tube Shielding. *J. Phys. Chem. C* **2008**, *112*, 11194-11198.
[67] Pfeiffer, R.; Pichler, T.; Kim, Y.; Kuzmany, H., in *Top. App. Phys.*, Vol. 111/2008, Springer Berlin / Heidelberg, **2008**.
[68] Pfeiffer, R.; Kuzmany, H.; Kramberger, C.; Schaman, C.; Pichler, T.; Kataura, H.; Achiba, Y.; Kürti, J.; Zólyomi, V. Unusual High Degree of Unperturbed Environment in the Interior of Single-Wall Carbon Nanotubes. *Phys. Rev. Lett.* **2003**, *90*, 225501-4.
[69] Liu, K.; Deslippe, J.; Xiao, F.; Capaz, R. B.; Hong, X.; Aloni, S.; Zettl, A.; Wang, W.; Bai, X.; Louie, S. G. An Atlas of Carbon Nanotube Optical Transitions. *Nat. Nanotechnol.* **2012**, *7*, 325-329.
[70] Ilev, I.; Waynant, R., in *Mid-Infrared Semiconductor Optoelectronics*, (Ed: Krier, A.), Springer Berlin, Heidelberg **2006**.
[71] Sandler, J.; Kirk, J.; Kinloch, I.; Shaffer, M.; Windle, A. Ultra-low electrical percolation threshold in carbon-nanotube-epoxy composites. *Polymer* **2003**, *44*, 5893-5899.
[72] Grady, B. P., *Carbon Nanotube-Polymer Composites: Manufacture, Properties, and Applications*, Wiley, **2011**.
[73] Flahaut, E.; Bacsa, R.; Peigney, A.; Laurent, C. Gram-Scale CCVD Synthesis of Double-Walled Carbon Nanotubes. *Chem. Commun.* **2003**, 1442-1443.
[74] Osswald, S.; Flahaut, E.; Gogotsi, Y. In situ Raman Spectroscopy Study of Oxidation of Double- and Single-Wall Carbon Nanotubes. *Chem. Mater.* **2006**, *18*, 1525-1533.
[75] Walsh, A. G.; Vamivakas, A. N.; Yin, Y.; Ünlü, M. S.; Goldberg, B. B.; Swan, A. K.; Cronin, S. B. Screening of Excitons in Single, Suspended Carbon Nanotubes. *Nano Lett.* **2007**, *7*, 1485-1488.
[76] Qian, H.; Georgi, C.; Anderson, N.; Green, A. A.; Hersam, M. C.; Novotny, L.; Hartschuh, A. Exciton Energy Transfer in Pairs of Single-Walled Carbon Nanotubes. *Nano Lett.* **2008**, *8*, 1363-1367.
[77] Förster, T. Transfer Mechanisms of Electronic Excitation. *Discuss. Faraday Soc.* **1959**, *27*, 7-17.
[78] Hayashi, T.; Shimamoto, D.; Kim, Y. A.; Muramatsu, H.; Okino, F.; Touhara, H.; Shimada, T.; Miyauchi, Y.; Maruyama, S.; Terrones, M. *et al* Selective Optical Property Modification of Double-Walled Carbon Nanotubes by Fluorination. *ACS Nano* **2008**, *2*, 485-488.

[79] Kim, J. H.; Kataoka, M.; Shimamoto, D.; Muramatsu, H.; Jung, Y. C.; Hayashi, T.; Kim, Y. A.; Endo, M.; Park, J. S.; Saito, R. *et al* Raman and Fluorescence Spectroscopic Studies of a DNA-Dispersed Double-Walled Carbon Nanotube Solution. *ACS Nano* **2010**, *4*, 1060-1066.
[80] Green, A. A.; Hersam, M. C. Processing and Properties of Highly Enriched Double-Wall Carbon Nanotubes. *Nat. Nanotechnol.* **2009**, *4*, 64-70.
[81] Tsyboulski, D. A.; Hou, Y.; Fakhri, N.; Ghosh, S.; Zhang, R.; Bachilo, S. M.; Pasquali, M.; Chen, L.; Liu, J.; Weisman, R. B. Do Inner Shells of Double-Walled Carbon Nanotubes Fluoresce? *Nano Lett.* **2009**, *9*, 3282-3289.
[82] Fantini, C.; Jorio, A.; Souza, M.; Strano, M. S.; Dresselhaus, M. S.; Pimenta, M. A. Optical Transition Energies for Carbon Nanotubes from Resonant Raman Spectroscopy: Environment and Temperature Effects. *Phys. Rev. Lett.* **2004**, *93*, 147406-4.
[83] Telg, H.; Maultzsch, J.; Reich, S.; Hennrich, F.; Thomsen, C. Chirality Distribution and Transition Energies of Carbon Nanotubes. *Phys. Rev. Lett.* **2004**, *93*, 177401-4.
[84] Meyer, J. C.; Paillet, M.; Michel, T.; Moreac, A.; Neumann, A.; Duesberg, G. S.; Roth, S.; Sauvajol, J. L. Raman Modes of Index-Identified Freestanding Single-Walled Carbon Nanotubes. *Phys. Rev. Lett.* **2005**, *95*, 217401-4.
[85] Kataura, H.; Kumazawa, Y.; Maniwa, Y.; Umezu, I.; Suzuki, S.; Ohtsuka, Y.; Achiba, Y. Optical Properties of Single-Wall Carbon Nanotubes. *Synth. Met.* **1999**, *103*, 2555-2558.
[86] Paillet, M.; Michel, T.; Meyer, J. C.; Popov, V. N.; Henrard, L.; Roth, S.; Sauvajol, J. L. Raman Active Phonons of Identified Semiconducting Single-Walled Carbon Nanotubes. *Phys. Rev. Lett.* **2006**, *96*, 257401-4.
[87] Jorio, A.; Saito, R.; Hafner, J. H.; Lieber, C. M.; Hunter, M.; McClure, T.; Dresselhaus, G.; Dresselhaus, M. S. Structural (n, m) Determination of Isolated Single-Wall Carbon Nanotubes by Resonant Raman Scattering. *Phys. Rev. Lett.* **2001**, *86*, 1118-1121.
[88] Araujo, P. T.; Doorn, S. K.; Kilina, S.; Tretiak, S.; Einarsson, E.; Maruyama, S.; Chacham, H.; Pimenta, M. A.; Jorio, A. Third and Fourth Optical Transitions in Semiconducting Carbon Nanotubes. *Phys. Rev. Lett.* **2007**, *98*, 067401-4.
[89] Villalpando-Paez, F.; Moura, L. G.; Fantini, C.; Muramatsu, H.; Hayashi, T.; Kim, Y. A.; Endo, M.; Terrones, M.; Pimenta, M. A.; Dresselhaus, M. S. Tunable Raman Spectroscopy Study of CVD and Peapod-Derived Bundled and Individual Double-Wall Carbon Nanotubes. *Phys. Rev. B* **2010**, *82*, 155416-9.
[90] Lazzeri, M.; Piscanec, S.; Mauri, F.; Ferrari, A. C.; Robertson, J. Phonon Linewidths and Electron-Phonon Coupling in Graphite and Nanotubes. *Phys. Rev. B* **2006**, *73*, 155426-6.
[91] Piscanec, S.; Lazzeri, M.; Robertson, J.; Ferrari, A. C.; Mauri, F. Optical Phonons in Carbon Nanotubes: Kohn Anomalies, Peierls Distortions, and Dynamic Effects. *Phys. Rev. B* **2007**, *75*, 035427-22.
[92] Ferrari, A. C.; Meyer, J. C.; Scardaci, V.; Casiraghi, C.; Lazzeri, M.; Mauri, F.; Piscanec, S.; Jiang, D.; Novoselov, K. S.; Roth, S. *et al* Raman Spectrum of Graphene and Graphene Layers. *Phys. Rev. Lett.* **2006**, *97*, 187401-4.
[93] Jorio, A.; Santos, A. P.; Ribeiro, H. B.; Fantini, C.; Souza, M.; Vieira, J. P. M.; Furtado, C. A.; Jiang, J.; Saito, R.; Balzano, L. *et al* Quantifying Carbon-Nanotube Species with Resonance Raman Scattering. *Phys. Rev. B* **2005**, *72*, 075207-5.
[94] Barros, E. B.; Son, H.; Samsonidze, G. G.; Souza Filho, A. G.; Saito, R.; Kim, Y. A.; Muramatsu, H.; Hayashi, T.; Endo, M.; Kong, J. *et al* Raman Spectroscopy of Double-Walled Carbon Nanotubes Treated with H_2SO_4. *Phys. Rev. B* **2007**, *76*, 045425-11.
[95] Cançado, L. G.; Jorio, A.; Ferreira, E. H. M.; Stavale, F.; Achete, C. A.; Capaz, R. B.; Moutinho, M. V. O.; Lombardo, A.; Kulmala, T. S.; Ferrari, A. C. Quantifying Defects in Graphene via Raman Spectroscopy at Different Excitation Energies. *Nano Lett.* **2011**, *11*, 3190-3196.
[96] Tuinstra, F.; Koenig, J. L. Raman Spectrum of Graphite. *J. Chem. Phys.* **1970**, *53*, 1126-1130.
[97] Ren, W.; Li, F.; Tan, P.; Cheng, H.-M. Raman Evidence for Atomic Correlation Between the two Constituent Tubes in Double-Walled Carbon Nanotubes. *Phys. Rev. B* **2006**, *73*, 115430-6.

[98] Bonaccorso, F.; Hasan, T.; Tan, P. H.; Sciascia, C.; Privitera, G.; Di Marco, G.; Gucciardi, P. G.; Ferrari, A. C. Density Gradient Ultracentrifugation of Nanotubes: Interplay of Bundling and Surfactants Encapsulation. *J. Phys. Chem. C* **2010**, *114*, 17267-17285.
[99] Hasan, T.; Scardaci, V.; Tan, P. H.; Rozhin, A. G.; Milne, W. I.; Ferrari, A. C. Stabilization and 'De-Bundling' of Single-Wall Carbon Nanotube Dispersions in N-Methyl-2-Pyrrolidone (NMP) by Polyvinylpyrrolidone (PVP). *J. Phys. Chem. C* **2007**, *111*, 12594-12602.
[100] Hasan, T.; Tan, P. H.; Bonaccorso, F.; Rozhin, A.; Scardaci, V.; Milne, W.; Ferrari, A. C. Polymer-Assisted Isolation of Single Wall Carbon Nanotubes in Organic Solvents for Optical-Quality Nanotube-Polymer Composites. *J. Phys. Chem. C* **2008**, *112*, 20227-20232.
[101] Cheng, Q. H.; Debnath, S.; Gregan, E.; Byrne, H. J. Effect of Solvent Solubility Parameters on the Dispersion of Single-Walled Carbon Nanotubes. *J. Phys. Chem. C* **2008**, *112*, 20154-20158.
[102] Travers, J. C.; Morgenweg, J.; Obraztsova, E. D.; Chernov, A. I.; Kelleher, E. J. R.; Popov, S. V. Using the E_{22} Transition of Carbon Nanotubes for Fiber Laser Mode-Locking. *Laser Phys. Lett.* **2011**, *8*, 144-149.
[103] Manzoni, C.; Gambetta, A.; Menna, E.; Meneghetti, M.; Lanzani, G.; Cerullo, G. Intersubband Exciton Relaxation Dynamics in Single-Walled Carbon Nanotubes. *Phys. Rev. Lett.* **2005**, *94*, 207401-4.
[104] Reich, S.; Dworzac, M.; Hoffmann, A.; Thomsen, C.; Strano, M. S. Excited-State Carrier Lifetime in Single-Walled Carbon Nanotubes. *Phys. Rev. B* **2005**, *71*, 03340-4.
[105] Cho, W. B.; Yim, J. H.; Choi, S. Y.; Lee, S.; Schmidt, A.; Steinmeyer, G.; Griebner, U.; Petrov, V.; Yeom, D.-I.; Kim, K. *et al* Boosting the Non Linear Optical Response of Carbon Nanotube Saturable Absorbers for Broadband Mode-Locking of Bulk Lasers. *Adv. Func. Mater.* **2010**, *20*, 1937-1943.
[106] Bohren, C. F.; Huffman, D. R., *Absorption and Scattering of Light by Small Particles*, Wiley-Interscience, New York **1998**.
[107] Agrawal, G. P., *Nonlinear fiber optics*, Academic Press, **2001**.
[108] Dennis, M. L.; Duling, I. N. Experimental Study of Sideband Generation in Femtosecond Fiber Lasers. *IEEE J. Quantum Electron.* **1994**, *30*, 1469-1477.
[109] Pandit, N.; Noske, D. U.; Kelly, S. M. J.; Taylor, J. R. Characterstic Instability of Fibre Loop Soliton Lasers. *Electron. Lett.* **1992**, *28*, 455-457.
[110] Von der Linde, D. Characterization of the Noise in Continuously Operating Mode-Locked Lasers. *Appl. Phys. B* **1986**, *39*, 201-217.
[111] Keller, U., in *Progress in Optics*, Vol. 46 (Ed: Wolf, E.), Elsevier, Amsterdam **2004**.